In the Proceedings of the IEEE conference on Computer Vision and Pattern Recognition, 2001

On the Perceptual Organization of Texture and Shading Flows: From a Geometrical Model to Coherence Computation *

Ohad Ben-Shahar
Department of Computer Science,
Yale university
New Haven, CT 06520-8285
ben-shahar@cs.yale.edu

Steven W. Zucker
Departments of Computer Science
and Electrical Engineering, Yale university
New Haven, CT 06520-8285
steven.zucker@yale.edu

Abstract

Locally parallel dense patterns - sometimes called texture flows *- define a perceptually coherent structure which is important to image segmentation, edge classification, shading analysis, and shape interpretation. This paper develops the notion of texture flow from a geometrical point of view to argue that* local *measurements of such structures must incorporate* two *curvatures. We show how basic theoretical considerations lead to a unique model for the local behavior of the flow and allow for the specification of consistency constraints between nearby measurements. The computation of* globally *coherent structure via neighborhood relationships is demonstrated on synthetic and natural images, and is compared to orientation diffusion.*

1. What is texture flow

A bear's fur, a zebra's stripes, and the wheat on a field all define a visual structure, sometimes called *texture flow*, whose organization to coherent parts is fundamental to many aspects of computer vision (Fig. 1). Informally, texture flows are defined by their orientation content - a dense visual percept characterized by local parallelism and *slowly* varying dominant local orientation (a.e.). The tendency of the human visual system to organize parallel structure has been observed psychologically [8, 2, 22], and its importance to computer vision has been discussed through the *non accidentalness* argument [26, 12]. For centuries this class of patterns has been used by artists as a tool to convey both the shape and shading of smoothly varying (continuous) surfaces and their discontinuities. Indeed, since the shading of smooth objects *is* a texture flow (e.g., when represented by its isoluminance contours), its analysis and segmentation in terms of coherent parts may prove vital for shape from shading (Fig. 2) and for edge classification [5].

Unfortunately, existing computational approaches to the analysis of texture flow, such as fitting [19] or diffusion [17, 21], ignore certain aspects of its structure. As a result, the processed flow may be distorted, especially around discontinuities (Fig. 2). Furthermore, the fact that coherent flow may contain a wide range of orientations within a small area takes its toll on segmentation methods (e.g., [11, 18]), leading to results that may disagree with perception (Fig. 3). We submit that the analysis of texture flow should be *geometrical* and should provide answers to two fundamental questions: (i) what should be measured locally, and (ii) how spurious measurements should be refined into globally coherent structures while *preserving discontinuities* and *singularities*. Since texture flows are perceptually dense even when the raw measurements are sparse, an adequate analy-

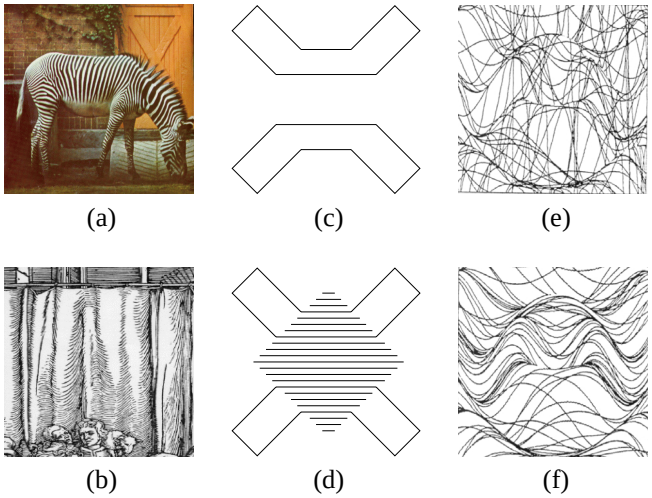

Figure 1: Instances of texture flows can be found in a variety of visual stimuli, both natural (a) and artificial (b). Furthermore, through what is known as the *social conformity of a line* [8], texture flows participate in perceptual organization to drastically affect our perception. Hence, while (c) is naturally perceived as two polygons, the superposition of (c) with a collection of parallel lines (d) is normally perceived as a diamond occluding a cross. Local parallelism is also important to the perception of shape. Although both (e) and (f) depict the same surface, its shape is apparent only when the set of surface contours possesses some degree of parallelism (reproduced from [22]).

*Supported by AFOSR. We deeply thank A. Tannenbaum for stimulating and inspiring discussions.

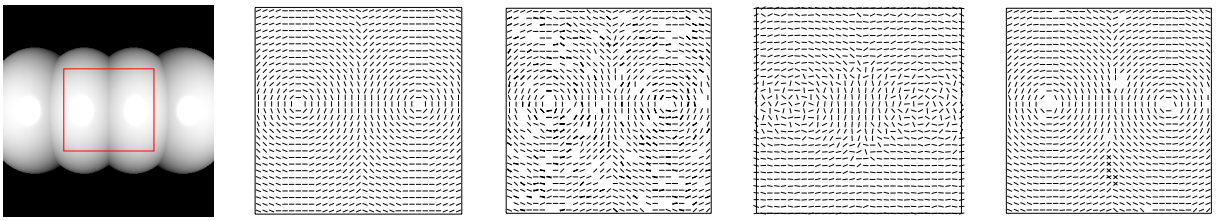

(a) (b) (c) (d) (e)

Figure 2: Since texture flows are commonly used to depict both shape and shading in drawings (as in Fig. 1(b)), we seek the common denominator between them. Indeed, virtually all piecewise smooth objects enjoy a shading flow which *is* a texture flow. (a) shows a worm-like object and a region of interest. (b) depicts the shading flow field (the tangent field to the isoluminance contours) of that ROI and (c) illustrates typical noisy measurements of that field. It is clearly essential that processing of this shading pattern preserves this structure, but current methods do not. For example, (d) shows the result of anisotropic orientation diffusion (Tang *et al.* [21], $P = 1$, step size = 0.1, 50 iterations) on that pattern. The structure is clearly distorted. On the other hand, the correct structure *is* preserved in (e), which shows the result of few iterations of our relaxation labeling process on the same input.

sis must *fill in* missing measurements. Since texture flows may overlap [24, 10], an appropriate approach should allow the representation of *multiple orientations* at a point. To our knowledge, no work to date possesses all these features.

While early attempts to address image parallelism computationally have focused on discrete representations [20], the dense characteristic of texture flow has shifted the focus to continuous representations. The importance of recovering the flow's *global structure* was argued by Kass and Witkin [9], who described a filtering method for extracting the flow's local orientation, but provided no robust method for the integration of the inherently noisy measurements. Shu and Jain [19] suggested estimating global texture flow structure through least squares fitting of the local orientation measurements to a first-order model (the phase portrait). While this averaging process can smooth noisy initial data, it can't handle discontinuities or overlapping flows. Orientation diffusion [17, 21] is an increasingly studied approach for the analysis of oriented patterns. Most recently, Tang *et al.* [21] proposed minimizing the harmonic energy of the pattern by flowing towards its critical points via gradient descent. Using different norms one can change the sensitivity of the diffusion to large scale discontinuities and hence the rate at which such structures in the orientation field are smoothed out. However, such anisotropic diffusion may fail to preserve essential structure (Fig. 2) and it is not designed to deal with missing measurements or overlapping flows.

2. A geometrical framework

The task of modeling texture flow coherence involves a few naturally related steps: one must decide on an appropriate representation, derive the necessary local features to be measured (the *measurements*), and model the way nearby coherent measurements fit together. These steps are studied in the following subsections.

2.1. Texture flow representation

A key step in any computation is a choice of representation [13]. Following our intuition in Section 1, texture flows can be naturally abstracted in one of few equivalent ways:

- a scalar orientation function $\theta(q)$ that defines the flow's dominant orientation at each point $q = (x, y)$.

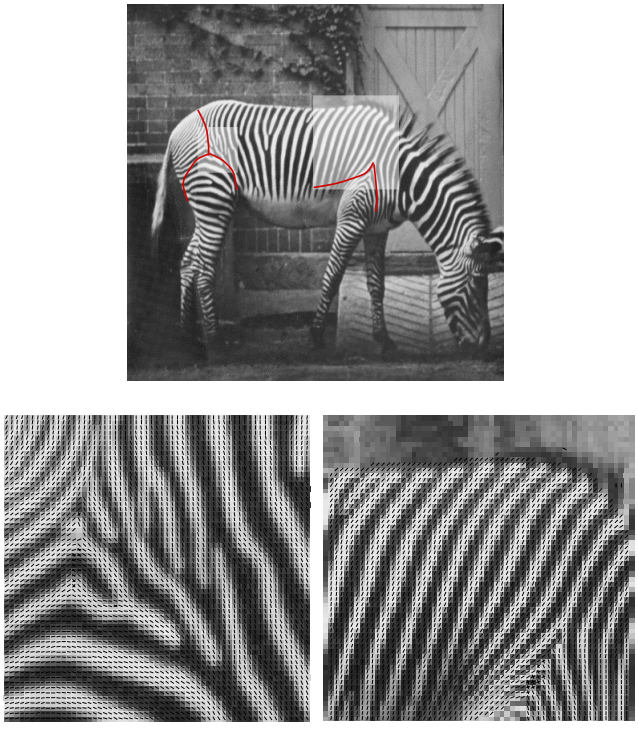

Figure 3: The fact that coherent flow may contain a wide range of orientations within a small area takes its toll on segmentation methods and affects their results. (Top) Two ROIs on a zebra image and an approximate manual segmentation as was computed in [18]. Note how the segmentation boundaries misrepresent the *single* underlying object. (Bottom) The corresponding texture flows computed by our system. Note that the structure is coherent almost everywhere, except at the properly isolated singularities.

- A 2D frame field [15] $E(q) = \{E_T(q), E_N(q)\}$ over the image plane. Naturally, we choose $E_T(q)$ as the unit vector field tangent to the flow, while $E_N(q)$ is the unit vector field normal to the flow.
- A 2D submanifold, or a surface in $R^2 \times S^1$. Since all our considerations are taken locally we will consider this representation to be the trace of a 2D height function $s(x, y) = (x, y, \theta(x, y))$ in R^3 whose Z axis represents orientation. We label this space by $XY\theta$.

While each representation makes explicit different properties of the object under investigation (e.g., the surface representation suggests the analysis of surface curvatures), they are completely equivalent in terms of their representational power. We make use of this equivalence below.

2.2. Texture flow local measurements

Part of the goal of modeling the local behavior of texture flow requires understanding the parameters that affect it. Taken as a scalar orientation function, the local behavior of the flow is governed to first order by its gradient. Unfortunately, this quantity is not naturally measurable from the image. The frame field representation provides an insightful alternative.

Taken as a frame field over the image plane, the local behavior of the flow is characterized by the differential behavior of the frame as it moves over the image plane. In particular, one may seek a representation of this behavior in terms of the frame itself, thus achieving an object-centered view which is invariant to Euclidean transformations (cf. Frenet frame and the Frenet equation for curves). This is captured by Cartan's *connection equations* [15]:

$$\begin{aligned} \nabla_V E_T &= \quad w_{12}(V) E_N \\ \nabla_V E_N &= -w_{12}(V) E_T \end{aligned} \tag{1}$$

where ∇_V is the *covariant derivative* in the direction V. The coefficient $w_{12}(V)$ is a function of the tangent vector V, which implies that the local behavior of the flow depends on the direction along which we measure it (Fig. 4). Fortunately, $w_{12}(V)$ is a *1-form* and thus linear. This allows us to fully represent it with two scalars since

$$w_{12}(V) = w_{12}(a\ E_1 + b\ E_2) = a\ w_{12}(E_1) + b\ w_{12}(E_2).$$

The freedom lies in choosing the basis to represent tangent vectors. In the flow-centered view, the natural choice is to set $E_1 = E_T$ and $E_2 = E_N$, defining the following two scalars :

$$\begin{aligned} \kappa_T &\stackrel{\triangle}{=} w_{12}(E_T) \\ \kappa_N &\stackrel{\triangle}{=} w_{12}(E_N) \end{aligned} \tag{2}$$

We call κ_T the *tangential curvature* and κ_N the *normal curvature* - they represent the rate of change of the dominant orientation of the texture flow in the tangential and normal directions, respectively. Based on a heuristic argument, Iverson [7] also used these curvatures. Because the tangential and normal directions are measurable in the image (based on the intensity gradient), we end up with a representation (κ_T, κ_N) of the differential behavior of the flow which is much more natural than its gradient[1]. Furthermore, since $\nabla\theta$ is also a 1-form, we can represent $w_{12}(V)$,κ_T, and κ_N all in terms of the appropriate projection:

$$\begin{aligned} \kappa_T &= \nabla\theta \cdot E_T = \nabla\theta \cdot (cos\theta, sin\theta) \\ \kappa_N &= \nabla\theta \cdot E_N = \nabla\theta \cdot (-sin\theta, cos\theta) \end{aligned} \tag{3}$$

Since E_T and E_N are rigidly coupled, we can rewrite Eq. 3 only in terms of E_T to yield the following relationships:

$$\begin{aligned} \kappa_T &= \nabla \times E_T \\ \kappa_N &= \nabla \cdot E_T \end{aligned} \tag{4}$$

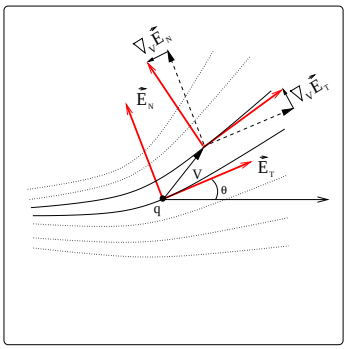

Figure 4: A texture flow can be represented as a differentiable frame field which is everywhere tangent (and normal) to the streamlines of the flow. An infinitesimal translation of the frame in a direction V rotates it by some angle determined by the connection form of the frame field. Since the connection form is a linear operator, it is fully characterized by two numbers obtained by the projection on two independent directions. It is a natural choice to use the directions defined by the frame itself, which yields the two curvatures κ_T and κ_N.

2.3. A Gestalt quality of texture flow

If κ_T and κ_N were known functions of position q, equation 3 could be viewed as a PDE and be solved for $\theta(q)$. This raises the question of the degree to which κ_T and κ_N are independent. Are they completely independent, as curvature and torsion are for curves, or are they dependent in the way the Gaussian and mean curvatures of surfaces are? We observe the following:

Proposition 1 *Unless κ_T and κ_N both equal zero, they cannot be simultaneously constant in a neighborhood around q, however small, or else the induced flow is non-integrable.*

[1]Note in particular that $\kappa_T(q)$ is just the curvature of the streamline passing through q.

This observation has an important implication: *In general, at least one of the curvatures must vary, or the two curvatures need to covary in any neighborhood of the texture flow*. This gestalt quality [25] of texture flow is formally characterized as follows:

Proposition 2 *Given any texture flow* $\{E_T, E_N\}$*, its curvature functions* κ_T *and* κ_N *must satisfy the relationship*

$$\nabla\kappa_T \cdot E_N - \nabla\kappa_N \cdot E_T = \kappa_T^2 + \kappa_N^2$$

2.4. Texture flow coherence

Since the local behavior of the flow is characterized (up to Euclidean transformation) by a pair of curvatures, it is natural to conclude that nearby local measurements of texture flow orientation should relate to each other based on these curvatures. Put differently, measuring a particular curvature pair $(\kappa_T(q), \kappa_N(q))$ at a point q should induce a field of coherent measurements (i.e., an orientation function $\theta(x, y)$) in the neighborhood of q. Clearly, that field, which we call the texture flow *osculating object*, should be a function of $(\kappa_T(q), \kappa_N(q))$. Coherence of local measurements of texture flow can then be determined in a manner analogous to cocircularity for tangents to a curve via the osculating circle [16].

Solving Eq. (3) with initial data at a single point q is equivalent to constructing the texture flow surface $s(x, y)$ (Sec. 2.1) given a single tangent plane at q. The set of possible solutions is infinite and the problem is underdetermined. We now make it well-posed by including the notion of "*slowly* varying dominant local orientation" (Sec. 1). We formalize this by introducing minimization constraints on the behavior of $\theta(x, y)$. But which one? The view of $\theta(x, y)$ as a 2D scalar function suggests looking for the critical points of the harmonic energy

$$\int\int ||\nabla\theta||^2 \, dxdy \tag{5}$$

in the spirit of Tang *et al.* [21]. On the other hand, the view of the flow as a surface suggests minimization of surface tension and looking for critical points of the area functional

$$\int\int \sqrt{1 + \theta_x^2 + \theta_y^2} \quad dxdy. \tag{6}$$

While each constraint individually is not sufficient to determine a unique solution to the construction problem, applying them *both* results in a surprising conclusion:

Proposition 3 *The solution for* $\theta(x, y)$ *satisfying the initial conditions at* q *and both constraints (5) and (6) is either*

$$\begin{array}{lrcl} \textit{a plane} & \theta(x,y) & = & K_T x + K_N y, \\ \textit{a right Helicoid} & \theta(x,y) & = & tan^{-1}(\frac{K_T x + K_N y}{1 + K_N x - K_T y}), \\ \textit{or a left Helicoid} & \theta(x,y) & = & tan^{-1}(\frac{K_T x + K_N y}{1 - K_N x + K_T y}). \end{array}$$

The proof is based on minimal surface theory [14] and on Hamel's theorem for harmonic minimal surfaces [3, 1].

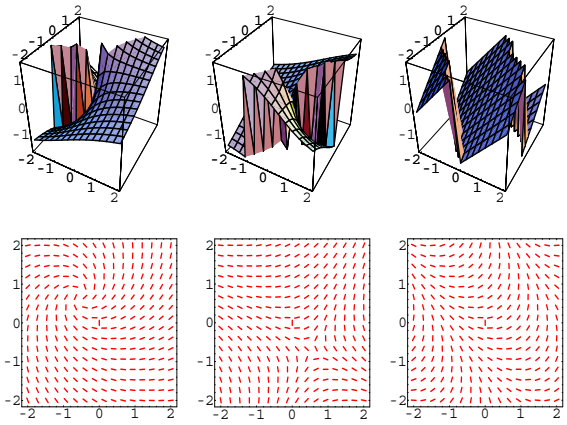

Right helicoid Left helicoid Plane

Figure 5: The only three solutions of Eq. 3 that are simultaneous critical points of the energy expressions (5) and (6), and that satisfy the initial conditions at q. We illustrate these three solutions for $\kappa_T(q) = 0.9$ and $\kappa_N(q) = 0.7$ both as surfaces in $XY\theta$ and their corresponding flows in the image plane. To set a visual context, we plot these solutions in a large neighborhood to show the singular point of the helicoids and the periodicity over the range $(-\frac{\pi}{2}, \frac{\pi}{2}]$.

The three solutions are visualized in Fig. 5. Naturally, all have the same tangent plane at q and one can show that the two helicoids even have identical local shape at q (i.e., the principle curvatures and directions of their surface representation coincide at q). Interestingly, they uniquely share another property:

Proposition 4 *The three solutions from Prop. 3 are the only functions (that satisfy the initial data and) whose p-Laplacian* $\Delta_P(\theta)$ *vanishes simultaneously for all* p*.*

This proposition reveals a formal relationship to [21] since it implies that each of the three functions is a stationary point of a gradient flow of the p-harmonic energy of the orientation function $\theta(x, y)$, regardless of the chosen metric p. While the theoretical consequences of this property remain to be analyzed, it reinforces the uniqueness of this set of solutions over others. Each of the three serves as a candidate *osculating object* for texture flow.

2.5. Curvatures covariation revisited

The discussion so far suggests two main observations with regard to the modeling and computation of coherent texture flow: (1) that texture flow measurements should include two curvature measurements (in addition to position and orientation), and (2) that nearby measurements should be considered coherent if they are part of (or "close" to) the same

osculating object. A question remains whether or not one of the three candidates is a better choice than the others.

As mentioned in Sec. 2.3, any nontrivial texture flow, and thus any osculating object, must incorporate some covariation of κ_T and κ_N around the point of measurement q. Representational and computational considerations dictate *simple* covariation; thus it is striking that

Proposition 5 *Of the three solutions of Prop. 3 (and of all orientation functions in general), the right helicoid has the "simplest" possible covariation of κ_T and κ_N since it is the only one to satisfy*

$$\frac{\kappa_T(x,y)}{\kappa_N(x,y)} = const = \frac{\kappa_T(q)}{\kappa_N(q)} \qquad \forall (x,y) \in N(q)$$

The fact that this behavior is unique to the helicoid can be derived from Eq. (3) by imposing constant covariation on κ_T and κ_N and reducing the system to a single quasi-linear differential equation

$$\vec{\mathbf{n}} \cdot (\kappa_N(q)cos\theta + \kappa_T(q)sin\theta, \kappa_N(q)sin\theta - \kappa_T(q)cos\theta, 0) = 0$$

where $\vec{\mathbf{n}}$ denotes a normal of the solution surface. One can then show that the characteristic curves of this PDE in $XY\theta$ constitute a ruling that defines a right helicoid.

The constant covariation of the two curvatures as induced by the right helicoid has an important computational advantage, since only one curvature (say, κ_T) needs to be explicitly maintained. The following section outlines how we use the right helicoid in a relaxation labeling network for the organization of texture flow.

3. Organization via relaxation labeling

The advantage of having a model for the local behavior of a "good" texture flow lies in the ability to assess the degree to which a particular measurement is compatible, or consistent, with the context in which it is embedded. This, in turn, can be used to refine noisy measurements, remove spurious ones, and fill in "holes" so that local ambiguity is reduced and global structures become coherent.

A natural framework with which one can pursue this task while maximizing the average consistency over a domain of interest is *relaxation labeling* [6]. We developed such a relaxation network for the organization of coherent texture flows and derived the compatibility function which governs its behavior from the right helicoidal model. The following is a short overview of that system, the details of which are described elsewhere.

A direct abstraction of the relaxation process for texture flow should involve an image-based 2D network of nodes $i = (x, y)$ (i.e., pixels) whose labels are drawn from the set

$$\Lambda = \{(\theta, \kappa_T, \kappa_N) \mid \theta \in (-\frac{\pi}{2}, \frac{\pi}{2}] \ , \ \kappa_T, \kappa_N \in [-K, K]\} \cup \text{no-flow}$$

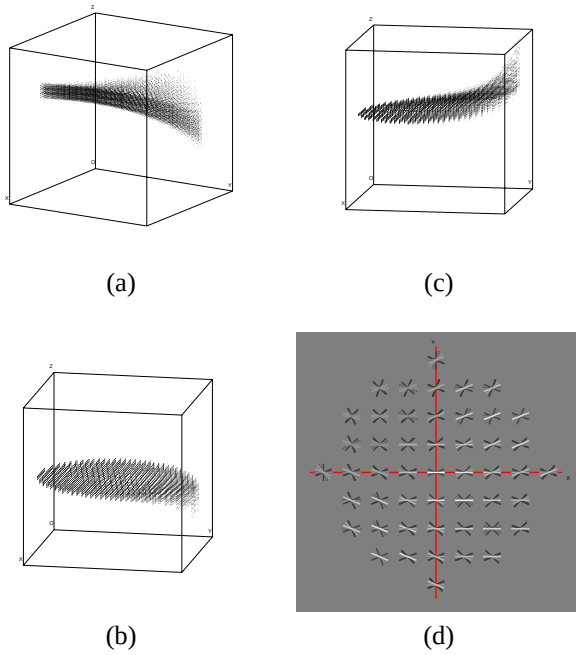

Figure 6: A visualization of the 5 dimensional consistency volume corresponding to particular measurements of θ, κ_T and κ_N at the origin. (a) shows the projection of that volume on $XY\theta$. (b) shows its projection on $XY\kappa_T$, and (c) shows its projection on $XY\kappa_N$. (d) depicts the projection of the consistency volume as orientation segments on the image plane (brightness represents degree of compatibility while the inhibitory surround is shown as black segments; see text).

after it has been quantized appropriately. Motivated by the columnar architecture of the visual cortex [4] and to allow for the representation of either "no-flow" or multiple flows at a pixel, we replace this abstraction with a 5D network of nodes $i = (x, y, \theta, \kappa_T, \kappa_N)$ whose labels are either $TRUE$ or $FALSE$. For each node i, $p_i(TRUE)$ denotes the confidence that a texture flow of orientation θ and curvatures κ_T, κ_N passes through pixel (x, y). Since $p_i(FALSE) = 1 - p_i(TRUE)$ we need to maintain and update the confidence of only one label at a node.

The geometrical compatibilities $r_{ij}(\lambda, \lambda')$ that drive our relaxation process are computed from the right helicoidal model. Measurements quantization implies that every possible node i represents an equivalence class of measurements, each of which induces a helicoidal field of compatible labels in the neighborhood of i. In the continuum, the union of all these fields forms a consistent 5D "volume" that after quantization results in a set of excitatory labels. Since the 5D relaxation network lacks an intrinsic normalization of labels at a position, we surround the excitatory region with an inhibitory surround (Fig. 6).

With the network structure, labels, and compatibilities all designed, one can compute the support $s_i(\lambda)$ that label

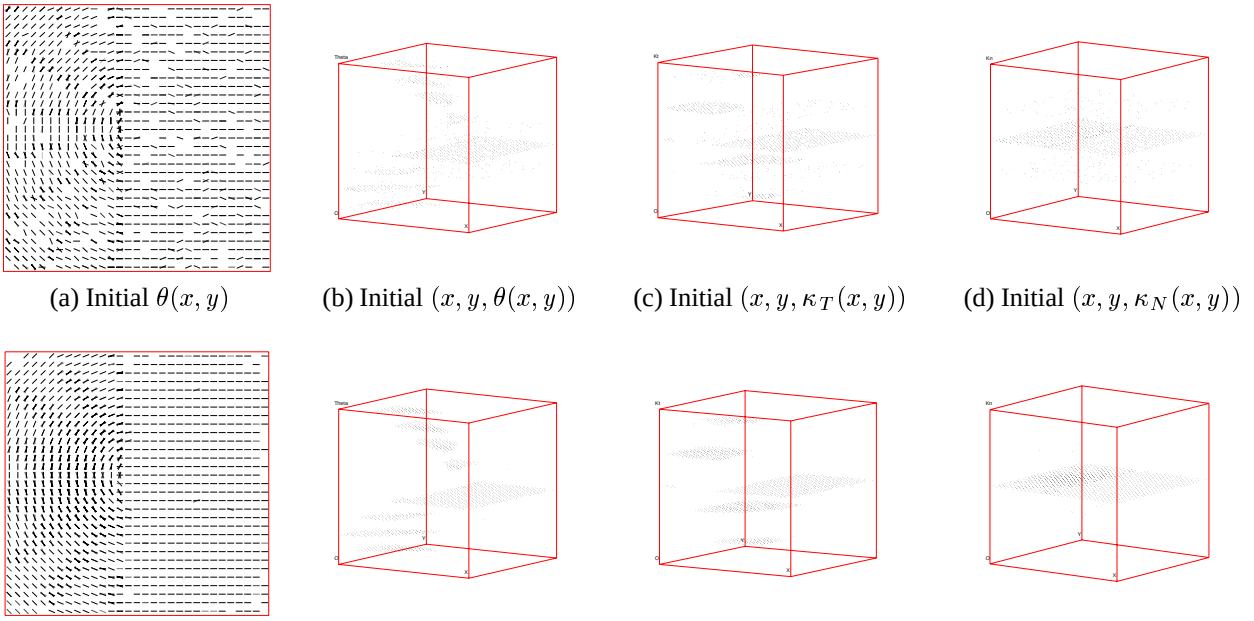

(a) Initial $\theta(x, y)$ (b) Initial $(x, y, \theta(x, y))$ (c) Initial $(x, y, \kappa_T(x, y))$ (d) Initial $(x, y, \kappa_N(x, y))$

(e) Relaxed $\theta(x, y)$ (f) Relaxed $(x, y, \theta(x, y))$ (g) Relaxed $(x, y, \kappa_T(x, y))$ (h) Relaxed $(x, y, \kappa_N(x, y))$

Figure 7: The organization of texture flow via relaxation labeling based on right helicoidal compatibilities. (a) is a noisy synthetic texture flow composed of two parts. Note that although the flow is almost everywhere continuous in terms of orientation, it is discontinuous in the tangential curvature along a vertical line. (b) depicts the initial distribution of orientation measurements while (c) and (d) illustrate the initial distribution of tangential and normal curvatures, respectively. Note that while the XY plane of (b)-(d) corresponds to the image plane, the Z axis represents either orientation (b), tangential curvature (c), or normal curvature (d). Sections (e) through (h) represent the corresponding distributions of labels' confidence after 10 iterations of relaxation labeling ($\delta = 0.25$). Missing measurements were filled in while noisy measurements were filtered out, making the entire structure globally coherent. Note that the discontinuity in tangential curvature *was not* smoothed out.

λ at node i gathers from its neighborhood. $s_i(\lambda)$ is typically the sum of the individual support of all labels j in the neighborhood of i,

$$s_i(\lambda) = \sum_j \sum_{\lambda'} r_{ij}(\lambda, \lambda') p_j(\lambda') \quad ,$$

and it can be designed to be stable at discontinuities or flow boundaries that cross i, i.e., it can support a coherent structure along one side of a discontinuity even when consistent measurements on its other side are lacking. Such $s_i(\lambda)$ is then used to update the confidence $p_i(\lambda)$ by gradient ascent followed by non-linear projection. Under the 2-label paradigm and an appropriate way of considering negative ($FALSE$) versus positive ($TRUE$) evidence, the projection operator takes a particularly simple form and the update rule reduces to

$$p_i(\lambda) \leftarrow \Pi_0^1 \left(p_i(\lambda) + \delta s_i(\lambda) \right)$$

where $\Pi_0^1(x)$ projects its operand to the nearest point on the interval $[0, 1]$ and δ is the step size of the gradient descent.

4. Experimental results

We tested the proposed model and relaxation system on a variety of inputs, both synthetic and natural. In all cases we quantized orientation to 16 equivalence classes and curvatures to 5. Figs. 7 to 9 show the results on synthetic flows. For such flows we computed exact initial measurements and then corrupted them along the orientation and curvature dimensions with additive and/or salt-and-pepper noise. Fig. 7 shows an example of a texture flow composed of two parts. Although the entire pattern is mostly continuous, there is a vertical line of discontinuity in the tangential curvature. Taken to be the flow underlying the shading on a bullet-like object, the preservation of such a discontinuity is of utmost importance since it indicates a second-order discontinuity in the observed shape, a property which may be used for part decomposition and object description. In this example, as in Figs. 8 and 9, the relaxation labeling process is able to eliminate the noise, to fill in holes, and to converge to a globally coherent structure while preserving the discontinuity. This counters the inherent limitation of orientation diffusion processes to represent *lack* of measurements (holes), flow boundaries (over which no oriented data exists) and multiple measurements (overlapping flows).

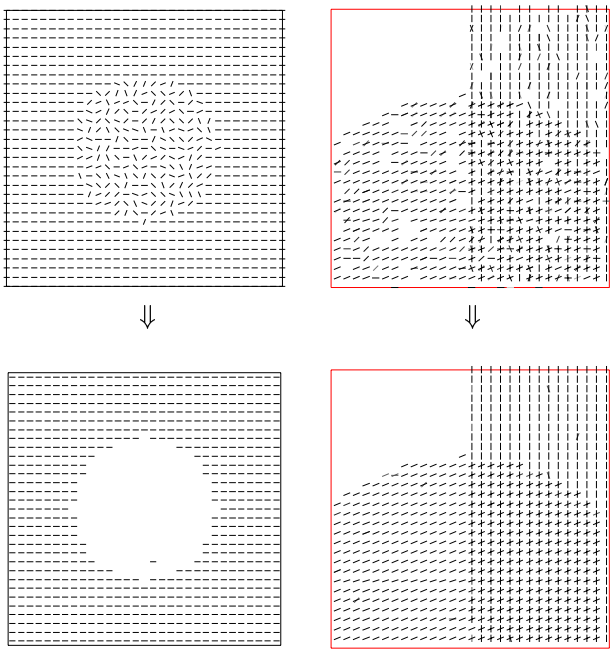

Figure 8: The organization of coherent structure based on right helicoidal compatibilities (20 iterations, $\delta = 0.25$). Note the removal of noisy measurements, the filling in of missing measurements, and the ability to cope with boundaries and overlapping flows. As opposed to orientation diffusion or averaging, non coherent structures are not relaxed to some meaningless average but rather are classified as non flows.

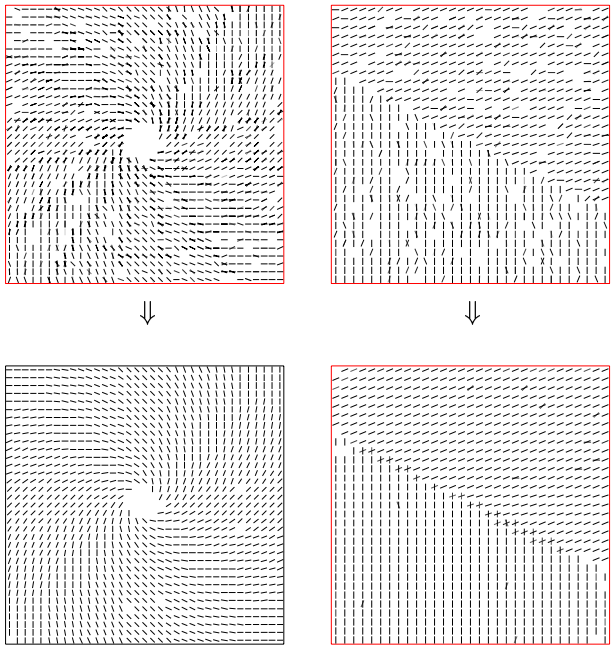

Figure 9: The organization of coherent flow structure based on right helicoidal compatibilities (20 iterations, $\delta = 0.25$).

Fig. 10 (also - Fig. 3) shows the results of applying our system to natural texture and shading flows. Initial measurements for these flows were computed directly from the image gradient orientation and application of Eq. (3). For texture flows (but not shading flows) we considered only high magnitude responses. Although this crude method of measuring flows provides very noisy curvature measurements, the relaxation process succeeded to extract the coherent structure. Note in particular how, in accordance with perception, the relaxation process successfully interpolates sparse texture flow measurements to a dense representation. In addition, note how non-flow structures are not smoothed to some meaningless average orientation, as orientation diffusion might do, but rather they are classified as no flows.

References

[1] W. Gaustein. Harmonic minimal surfaces. In *Trans. of the American Mathematical Society*, volume 47, pages 173–206, 1940.

[2] L. Glass. Moiré effect from random dots. *Nature*, 223(5206):578–580, 1969.

[3] G. Hamel. Zum gedachtnis an hermann amandus schwarz. *Jahresber, D.M.V.*, 32:6–13, 1923.

[4] D. Hubel and T. Wiesel. Functional architecture of macaque monkey visual cortex. In *Proc. of the Royal Society (London) B*, volume 198, pages 1–59, 1977.

[5] P. Huggins and S. Zucker. How folds cut a scene. In *Proc. of the* 4^{th} *Int. Workshop on Visual Form*, 2001.

[6] R. Hummel and S. Zucker. On the foundations of the relaxation labeling proceeses. *IEEE Trans. on Pattern Analysis and Machine Intelligence (PAMI)*, 5:267–287, 1983.

[7] L. Iverson. *Toward Discrete Geometric Models for Early vision*. PhD thesis, McGill University, 1994.

[8] G. Kanizsa. *Organization in Vision: Essays on Gestalt Perception*. Praeger Publishers, 1979.

[9] M. Kass and A. Witkin. Analyzing oriented patterns. *Computer Vision, Graphics and Image Processing*, 37:362–385, 1987.

[10] D. Keeble, F. Kingdom, and M. Morgan. The orientational resolution of human texture perception. *Vision Research*, 37(21):2993–3007, 1997.

[11] T. Lee. A bayesian framework for understanding texture segmentation in the primary visual cortex. *Vision Research*, 35(18):2643–2657, 1993.

[12] D. Lowe. *Perceptual Organization and Visual Recognition*. Kluwer Academic Publishers, 1985.

[13] D. Marr. *Vision*. W.H.Freeman and Company, 1982.

[14] J. Nitsche. *Lectures on Minimal Surfaces*. Cambridge Univ. Press, 1989.

[15] B. O'Neill. *Elementary Diff. Geom.* Academic Press, 1966.

[16] P. Parent and S. Zucker. Trace inference, curvature consistency, and curve detection. *IEEE Trans. on Pattern Analysis and Machine Intelligence (PAMI)*, 11(8):823–839, 1989.

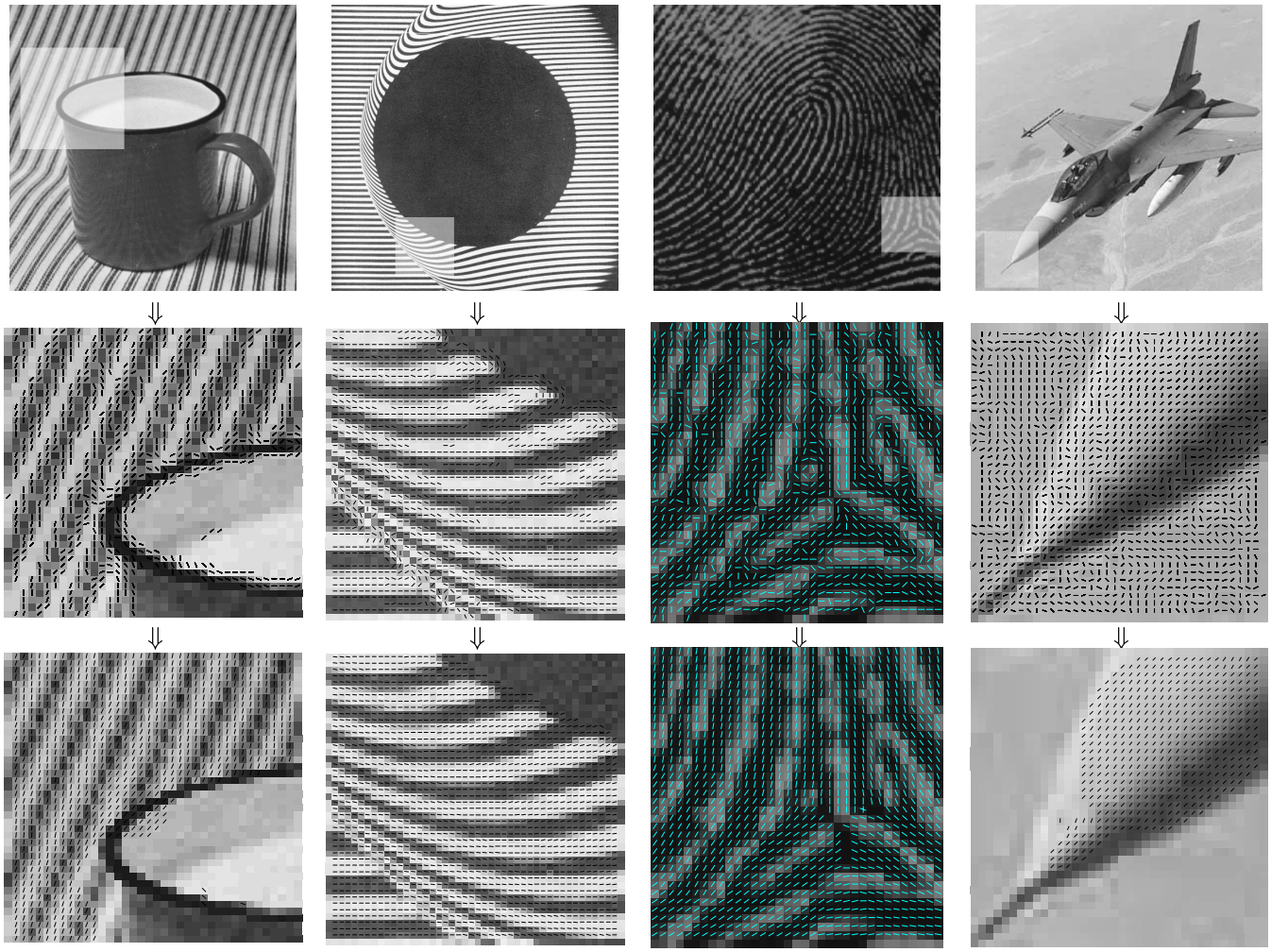

Figure 10: Natural texture (a-b) and shading (c-d) flow organization based on right helicoidal compatibilities. Top row shows the raw intensity images and a region of interest to which we applied the relaxation process. Middle row shows the initial measurements superimposed on the intensity ROI. Bottom row shows the resultant flows. (a) is a photo of a cup on a table cover. Note how the process fills in the many missing measurements to create a dense and coherent representation. (b) is a fluid flow photo from [23]. Note how the flow discontinuity is preserved in the result. (c) is a fingerprint image for which the system is given a dense but noisy field of gradient based shading measurements. Along with preserving the singularity, the result is a coherent field that agrees with the underlying perceptual structure. (d) is a photo of F16. Our system was able to organize the coherent shading flow on the plane's nose while suppressing the non coherent structure at the background. Such an organization is particularly useful for edge classification [5] and further shading analysis.

[17] P. Perona. Orientation diffusion. *IEEE Trans. on Image Processing*, 7(3):457–467, 1998.

[18] J. Shi and J. Malik. Normalized cuts and image segmentation. In *Proc. of the IEEE Conf. on Computer Vision and Pattern Recognition (CVPR)*, 1997.

[19] C. Shu and R. Jain. Direct estimation and error analysis for oriented patterns. *Computer Vision, Graphics and Image Processing*, 58(3):383–398, 1993.

[20] K. Stevens. Computation of locally parallel structure. *Biological Cybernetics*, 29:19–28, 1978.

[21] B. Tang, G. Sapiro, and V. Caselles. Diffusion of general data on non-flat manifolds via harmonic maps theory: The direction diffusion case. *Int. J. of Computer Vision*, 36(2):149–161, 2000.

[22] J. Todd and F. Reichel. Visual perception of smoothly curved surfaces from double-projected contour patterns. *J. Exp. Psych.: Human Perception and Performance*, 16(3):665–674, 1990.

[23] M. Van Dyke. *An Album of Fluid Motion*. The Parabolic Press, 1982.

[24] T. Watanabe and P. Cavanagh. Texture laciness: The texture equivalent of transparancy? *Perceeption*, 25:293–303, 1996.

[25] M. Wertheimer. Gestalt theory. In W. Ellis, editor, *A source book of Gestalt Psych.*, pages 1–11. Routledge & Kegan Paul Ltd., 1955.

[26] A. Witkin and J. Tenenbaum. On the role of structure in vision. In J. Beck, B. Hope, and A. Rosenfeld, editors, *Human and Machine Vision*, pages 481–542. Academic Press, 1983.